Journal of Environmental Chemical Engineering 14 (2026) 125663

Contents lists available at ScienceDirect

Journal of Environmental Chemical Engineering

journal homepage: www.elsevier.com/locate/jece

Mechanistic insights into chain-length dependent PFOA and PFBS adsorption on polyethyleneimine-functionalized fibrous silica aerogels

Jai Kishan Rajak [a], G.V. Koulini [b], Indumathi M. Nambi [b,c], Sulalit Bandyopadhyay [a,*]

[a] Particle Engineering Centre, Department of Chemical Engineering, Norwegian University of Science and Technology, Trondheim, 7491, Norway
[b] Environmental Engineering Division, Department of Civil Engineering, Indian Institute of Technology Madras, Chennai, Tamil Nadu 600036, India
[c] School of Sustainability, Indian Institute of Technology Madras, Chennai, Tamil Nadu 600036, India

ARTICLE INFO

Keywords:
PFAS adsorption
Polyethyleneimine
Silica aerogel
PFOA
PFBS
Water matrices
Desorption and reusability
Electrostatic interaction

ABSTRACT

Per- and polyfluoroalkyl substances (PFAS) are persistent environmental contaminants linked to adverse health outcomes and are difficult to remove from water because of their chemical stability and structural diversity. In this study, a polyethyleneimine (PEI)-functionalized mesoporous silica aerogel was developed to investigate how PFAS structure and water chemistry affect adsorption under controlled batch conditions. Silica aerogels were synthesized via a microemulsion-assisted sol–gel method to produce highly porous networks and subsequently modified with PEI to introduce protonatable amine groups. At the same PEI loading (50 wt%), the lower-molecular-weight PEI_{600} aerogel retained a higher BET surface area and pore volume than the $PEI_{25,000}$ aerogel (162 vs. 78 m^2/g and 0.9 vs. 0.5 cm^3/g), and showed the higher PFAS adsorption performance. Adsorption behavior was evaluated using perfluorooctanoic acid (PFOA) and perfluorobutanesulfonic acid (PFBS) as model long- and short-chain PFAS. Rapid uptake occurred for both compounds, with equilibrium reached within 60–120 min. Equilibrium studies showed consistently greater adsorption of PFOA than PFBS. Freundlich isotherm modeling provided the best overall fit, indicating heterogeneous adsorption behavior, while PFOA showed greater adsorption than PFBS across the investigated conditions. Adsorption decreased with increasing pH and ionic strength, with PFBS showing greater sensitivity to these conditions. In treated sewage effluent, PFOA removal remained relatively high (~70%), whereas PFBS removal declined to ~30–37%, underscoring the stronger matrix effects on short-chain PFAS. Desorption and reusability tests using of 1% NaCl in 80% methanol preserved approximately 88% and 75% of adsorption efficiency for PFOA and PFBS, respectively, after five cycles. X-ray photoelectron spectroscopy supported PFAS retention on PEI-modified surfaces, with changes in nitrogen chemical states following adsorption. These findings highlight the role of PEI accessibility and PFAS chain length in controlling adsorption on fibrous silica aerogels and provide guidance for the design of amine-functionalized PFAS sorbents.

1. Introduction

Per- and polyfluoroalkyl substances (PFAS) represent a large class of persistent environmental contaminants that have become a global concern due to their high chemical stability, environmental persistence, mobility, and associated adverse health impacts [1–3]. More than 12,000 synthetic PFAS have been identified, characterized by a highly fluorinated carbon backbone and diverse terminal functional groups [1,4]. Due to their unique amphiphilic character and the strength of the carbon–fluorine bond, PFAS have been widely employed across a wide range of applications, including industrial processes, mining, food packaging, and fire-fighting foams [5]. Human exposure can occur through contaminated water, food, dust, and other environmental pathways, and has been associated with several adverse health outcomes [6–8]. As a consequence of their extensive use and environmental persistence, PFAS are now detected in groundwater, surface waters, drinking water, soils, sediments, rainwater, indoor air, and biota, even in remote ecosystems [9]. This widespread occurrence highlights the urgent need for effective strategies to remove PFAS from contaminated water.

Long-chain PFAS such as perfluorooctanoic acid (PFOA) and perfluorooctanesulfonic acid (PFOS) were extensively used throughout the

* Corresponding author.
E-mail address: sulalit.bandyopadhyay@ntnu.no (S. Bandyopadhyay).

https://doi.org/10.1016/j.jece.2026.125663
Received 21 July 2026; Received in revised form 8 October 2026; Accepted 25 October 2026
Available online 26 October 2026
2213-3437/© 2026 The Author(s). Published by Elsevier Ltd. This is an open access article under the CC BY license (http://creativecommons.org/licenses/by/4.0/).

mid-20th century [10]. With PFOS listed in 2009 and PFOA in 2019) being listed under the Stockholm Convention for global phase-out, the use and detection of several short-chain and replacement PFAS have increased [11]. In the European Union, PFASs in drinking water are primarily regulated under Directive (EU) 2020/2184 (recast Drinking Water Directive), which establishes a parametric value of 0.50 μg/L for the "PFAS Total" parameter, defined as the aggregate concentration of all PFASs in water intended for human consumption [12]. PFAS have been reported across a wide concentration range in surface water, groundwater, wastewater, and drinking-water sources, depending on source strength, site history, and hydrological setting [13–15]. Field sampling studies, such as those by Schroeder *et al.*, have reported PFOA concentrations up to 100 ng/L in groundwater-connected springs [16]. Short-chain PFAS (e.g., PFBS) have increased in use as replacements for phased-out long-chain compounds used in textiles, pharmaceuticals, food packaging, and cleaning products [12,17]. Therefore, comparing PFOA and PFBS provides a useful basis for examining how PFAS chain length and headgroup chemistry influence adsorption on functionalized sorbents. Despite expanding research, significant challenges persist in PFAS remediation. Many adsorption and ion-exchange materials lose efficiency in high ionic strength or natural water matrices, show lower affinity for short-chain PFAS, and show performance that depends strongly on PFAS chain length, functional group chemistry, and background water composition [18]. Although numerous materials have been investigated from traditional activated carbons and ion-exchange resins to metal–organic frameworks and polymer composites, direct comparison remains difficult as the reported studies often differ in initial experimental conditions, and whether adsorption is evaluated under batch or flow conditions. These challenges have also been highlighted in recent reviews on PFAS adsorption and sorbent design [19,20]. To place our findings in context with closely related sorbents, Table S6 compares selected materials reported for PFOA and PFBS adsorption, including their testing conditions and adsorption performance. Because these studies differ in concentration range, pH, contact time, sorbent dose, and water matrix, the comparison is used to contextualize the present material rather than to imply a direct head-to-head benchmark. This highlights the need for systematic studies that resolve fundamental interactions under controlled aqueous environments, particularly when comparing long- and short-chain PFAS.

Functional modification of porous inorganic matrices with amine-rich polymers offers a promising strategy to address these gaps [21]. Polyethyleneimine (PEI)-functionalized adsorbents have shown strong potential for PFAS removal due to their ability to interact with anionic headgroups [22]. Although some studies have explored PEI-functionalized materials for PFAS adsorption, a key design question remains: how does the support architecture control PEI accessibility and the availability of protonatable amine sites? To address this, we introduce a modified microemulsion-assisted sol–gel synthesis that produces a fibrous silica aerogel framework with an open, interconnected porous morphology. Unlike conventional mesoporous silica (e.g MCM-41, SBA-15, KIT etc.) or dense silica–PEI composites, this aerogel structure provides high pore volume, large surface area, and connected mesoporous pathways that can facilitate PEI incorporation while maintaining access to amine-rich regions of the sorbent. Together, these features position PEI-modified aerogels as an effective platform for systematic structure–function studies in PFAS adsorption. We hypothesize that the fibrous silica aerogel architecture improves the accessibility of PEI-derived amine sites, and that this accessibility depends on PEI molecular weight Specifically, lower-molecular weight PEI is expected to preserve pore access more effectively than higher-molecular weight PEI. We further hypothesize that PFOA will adsorb more strongly than PFBS due to its longer perfluoroalkyl chain providing additional non-electrostatic contributions, whereas PFBS adsorption will be more sensitive to solution conditions (pH, ionic strength, and background constituents). To examine these effects, adsorption kinetics and equilibrium behavior are evaluated under systematically varied pH and ionic strength conditions, alongside desorption and reusability over multiple adsorption–desorption cycles. Adsorption behavior is further assessed in natural water matrices to evaluate the influence of background constituents. Further, X-ray photoelectron spectroscopy (XPS) was employed for interpretation of the dominant interactions involved in PFAS uptake, providing chemical context for the observed adsorption trends rather than definitive mechanistic proof. Overall, this study aims to clarify how aerogel pore architecture, PEI accessibility, and PFAS molecular structure collectively influence adsorption behavior under controlled batch conditions.

2. Materials and methods

2.1. Materials

All reagents were of analytical grade and used without further purification. Cetyltrimethylammonium bromide (CTAB, 99%), polyethyleneimine (PEI; MW ≈ 600 Da and 25,000 Da), tetraethyl orthosilicate (TEOS, 99%), triethanolamine (≥99.5%), ethanol (≥99%), toluene (99%), nonafluorobutane-1-sulfonic acid (98%), perfluorooctanoic acid (95%), and ammonium acetate (≥97%) were obtained from Sigma-Aldrich. Hydrochloric acid (HCl, 37%) and sodium hydroxide (NaOH, ≥99%) were purchased from Thermo Fisher Scientific. Sodium chloride (NaCl, ≥99%) was purchased from Merck, and LC–MS-grade methanol was obtained from Actylis Lab Solutions. All solutions were prepared using DI-water (18.2 MΩ·cm resistivity). Centrifuge tubes (50 mL), and pipette tips (200 μL, 1 mL, and 5 mL) were purchased from Tarsons Products Ltd, and LC-MS autosampler 2 mL vials and screw caps were purchased from Agilent, all made of polypropylene.

2.2. Synthesis of Silica Aerogels

Silica aerogel was synthesized using a microemulsion-assisted sol–gel approach. The procedure was adapted with modifications from the method reported by Polshettiwar *et al.* [23]. In a typical synthesis, 2.7 g of cetyltrimethylammonium bromide (CTAB) was dissolved in 120 mL of Milli-Q water under stirring (600 rpm) for 35–40 min, followed by the addition of 2.0 Ml of triethanolamine (TEA). Separately, an organic mixture containing 6.8 mL of tetraethyl orthosilicate (TEOS), 4.0 mL of 1-butanol, and 90 mL of toluene was prepared and added dropwise to the aqueous solution under vigorous stirring (800 rpm) to form a stable emulsion. The resulting mixture was refluxed at 110°C for 16 h to facilitate hydrolysis and condensation of TEOS around the CTAB micelles. After cooling, the solid product was collected by centrifugation, washed twice with ethanol, and dried at 70 °C overnight. The obtained material was calcined at 550 °C for 5 h in air to remove the surfactant template, yielding the mesoporous silica aerogel.

2.3. Fabrication of Polyethyleneimine (PEI) on silica aerogels

Before the functionalization process, the aerogel was first crushed into a fine powder and pre-dried at 250 °C for 30 min to remove physisorbed moisture. The functionalization procedure was adapted from the work of Doan *et al.* [24]. In brief, separate methanolic solutions of PEI_{600} and $PEI_{25,000}$ were prepared and stirred for 20 min at room temperature. The dried silica powder was then dispersed in the corresponding PEI–methanol solution, and the mixture was maintained at 45 °C under continuous stirring for 6 h to allow physical impregnation of PEI within the silica pore network. The PEI:silica aerogel ratio was maintained at 1:1 (w/w), corresponding to a nominal PEI loading of 50 wt%. The solvent was subsequently removed under reduced pressure (6–32 kPa), and the material was vacuum-dried at 65 °C for at least 16 h. The resulting PEI-functionalized silica aerogels were stored in capped bottles until further use.

2.4. Characterization

Sorbents were synthesized in multiple batches and combined into a single homogeneous batch for all sorption and characterization studies. Morphology was examined using a JEOL 300 kV high-resolution transmission electron microscope (HR-TEM), with samples drop-cast onto carbon film–coated copper grids. The zeta potential was measured by making a suspension of the aerogel particles (300 mg L^{-1} in water) using a LiteSizer 500 (Anton Paar). Surface functional groups were characterized by Fourier-transform infrared spectroscopy (FTIR, Bruker Alpha-Platinum ATR) at a resolution of 2 cm^{-1} with 100 scans on dried samples. Following this, Thermogravimetric analysis (TGA, Netzsch-Gerätebau GmbH, Germany) was conducted using a TA Instruments system, with samples heated to 900 °C at 10 °C min^{-1} under nitrogen. Additional TGA measurements were performed on aerogels recovered after exposure at pH 3, 6.5, and 9 and after the first and fifth adsorption–desorption cycles to assess changes in the PEI-associated organic fraction following aqueous exposure and repeated reuse (Figure S5). Surface chemistry before and after adsorption of the dried sorbent was determined by X-ray photoelectron spectroscopy (XPS, ThermoScientific K-Alpha) employing an Al Kα X-ray source. For XPS analysis, dried samples were mounted on carbon tape prior to measurement. Metal quantification was carried out using an Agilent 4210 Microwave Plasma–Atomic Emission Spectrometer (MP-AES). Samples were diluted in 2% HNO_3 and analyzed in triplicate. Calibration curves were prepared by diluting a 1000 mg L^{-1} multi-element standard solution (Certipur®). Instrumental uncertainty was assessed by analyzing calibration standards as samples, with an average deviation below 2%.

2.5. Adsorption experiments

Batch adsorption experiments were performed to evaluate the removal of PFOA and PFBS using synthesized PEI-silica aerogels. Stock solutions (100 mg L^{-1}) of each PFAS were prepared from solid standards and diluted to the desired concentrations (0.1–1 mg L^{-1}). Adsorption experiments were performed in 50 mL centrifuge tubes containing 10 mg of aerogel and 40 mL of PFAS solution, agitated at 150 rpm and maintained at 299 K across a pH range of 3–9. Aliquots collected at predetermined intervals (ranging from 0.08 to 24 hrs) were used to measure sorption kinetics. Conversely, equilibrium isotherms were constructed by systematically modulating the initial PFAS concentration with 24 hrs contact time. The equilibrium data were fitted using the Langmuir, Freundlich, Sips, and Temkin isotherm models, while kinetic data were evaluated using the pseudo-first order (PFO), pseudo-second order (PSO), general-order (GO), and Weber–Morris intraparticle diffusion models. The corresponding equations are provided in Table S5. Apparent thermodynamic parameters (ΔG°), (ΔH°), and (ΔS°) were estimated from the temperature-dependent equilibrium data using the van't Hoff relationship. To assess the influence of water chemistry, we investigated the effects of pH, ionic strength, and diverse water matrices. Several desorption agents were screened, and the best-performing regenerant was subsequently evaluated over repeated adsorption–desorption cycles. Error bars in the kinetic and isotherm plots represent the standard deviation of triplicate measurements, while experiments examining pH, ionic strength, water matrices, and reusability were performed in duplicates.

2.6. Analytical methods and calculations

The samples (1 mL) collected from conical tubes were centrifuged for 15 min at 12,000 rpm. The supernatant was collected in the LC-MS autosampler vials and analyzed using Shimadzu make iSeries plus High-Performance Liquid Chromatography (HPLC) with Photodiode Array (PDA) detector and triple quad mass spectrometer - LCMS 8040. Chromatographic separation was achieved using a C18 column (4.6 ×250 mm, 5 μm). 20 mmol/L ammonium acetate and 100% methanol were used as mobile phases A and B, respectively, with a 0.8 mL/min solvent flow rate. The analysis was carried out in multiple reaction monitoring (MRM) with a negative electron spray ionization mode for a run time of 20 min. The chromatographic separation was carried out using a gradient elution program as follows: the mobile phase B was maintained at 70% from 0.01 to 8 min, then increased linearly to 95% at 9 min and held constant at 95% until 12 min. The mobile phase B was then decreased back to 70% at 13 min, maintained at 70% until 18 min, and the run was stopped at 20 min. The injection volume was 10 μL. The other conditions were column temperature 40 °C, desolvation line (DL) & heatblock (HB) temperature 250 °C and 400 °C respectively, and nebulizing gas flow N_2) 2.8 mL/min.

Quantitation of both PFOA and PFBS was accomplished using three separate calibration curves, each consisting of six points within the concentration ranges 1–10 μg/L, 10–100 μg/L, and 100–1000 μg/L. All curves demonstrated a linear regression coefficient (r^2) of $\geq$ 0.99 for both PFOA and PFBS. Limit of quantification (LOQ) is 1 μg/L for both the analytes. Individual 1000 mg/L stock standard solutions of PFOA and PFBS were prepared in methanol and serially diluted in 100% methanol to obtain the required calibration standards (Figure S3).

The percentage removal was determined using the following equation:

$$Removal, \% = \frac{C_0 - C}{C_0} x100$$

In this equation, C_0 and C are the initial and final concentrations of PFOA/PFBS in water.

3. Results and discussion

3.1. Characterization of adsorbent

3.1.1. Structural characterization

High-resolution TEM was used to examine whether the fibrous aerogel morphology was retained after PEI functionalization. The pristine silica aerogel (Fig. 1**a**), imaged at a 100 nm scale, revealed an open, sheet-like porous network composed of ultrathin, wrinkled silica layers. In the high resolution (scale-10 nm) inset, these sheets appeared as mono- to multi-layered sheets, with visibly interconnected void spaces and a fragmented architecture, typical signature of low-density silica aerogels synthesized under base-catalyzed sol–gel conditions. Additionally, zoomed image-inset shows a more magnified (scale 10 nm) the physical appearance of both the pristine and PEI-functionalized aerogels, are provided in Figure S2 of the Supplementary Information. Similar morphological characteristics have previously been reported, describing silica aerogels as loosely aggregated networks of nanostructured silica ridges and lamellar domains [25–27].

After PEI functionalization, the overall aerogel framework was largely retained, although textural changes were evident (Fig. 1**b**). The PEI-modified sample appears denser and less transparent in several regions, indicative of polymer incorporation and partial pore fillings. Such compaction effects have been similarly observed in PEI-modified silica and alumina porous systems, where amine-rich polymer layers hold strongly to surface hydroxyl groups, altering local electron density and decreasing pore openness [27]. These morphological observations provide qualitative evidence of changes following PEI functionalization. BET analysis was therefore performed to further evaluate changes in the textural properties.

3.1.1.1. Surface Textural Properties. Nitrogen adsorption–desorption isotherms for the pristine and PEI-functionalized silica aerogels (Fig. 1**c**) display type IV behavior with pronounced hysteresis loops, confirming retention of the mesoporous structure after PEI incorporation. The corresponding BET surface area, average pore size, and pore volume are summarized in Table 1.

PEI incorporation substantially reduced the surface area and pore

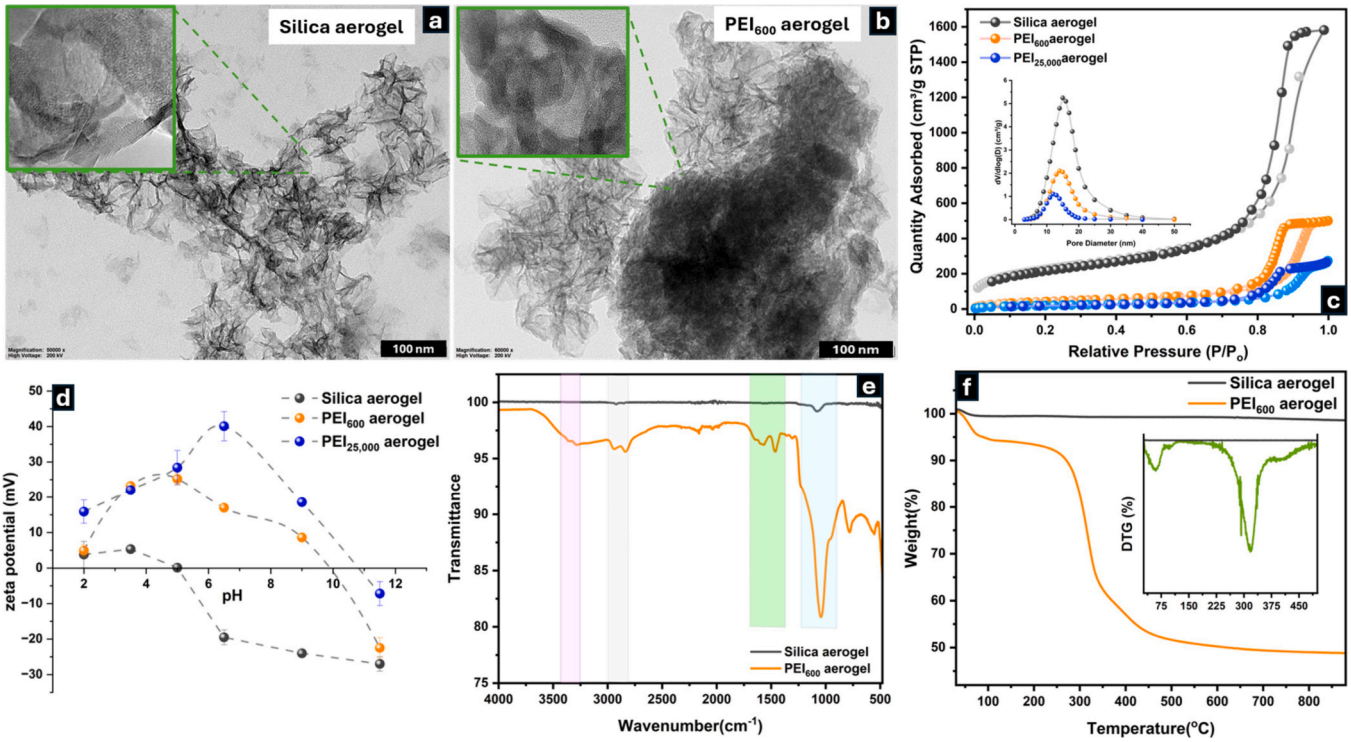

Fig. 1. *High-resolution TEM images of (a) pristine aerogel and (b) PEI_{600} aerogel at a scale of 100 nm, with higher-resolution images shown in the insets (scale: 10 nm); (c) N_2 adsorption–desorption isotherms with the corresponding pore-size distributions shown in the inset; (d) zeta potential as a function of pH; (e) FTIR spectra; and (f) TGA curves showing the thermal degradation profiles of the aerogels.*

Table 1
Textural properties of pristine and PEI-functionalized silica aerogels.

Sample	BET area (m^2/g)	Average pore size (nm)	Pore volume (cm^3/g)
Silica aerogel	788	15.5	2.6
PEI_{600}–aerogel	162	18.1	0.9
$PEI_{25,000}$-aerogel	78	19.1	0.5

volume, with a greater reduction for $PEI_{25,000}$ than for PEI_{600}, indicating stronger restriction of the pore network by the higher-molecular-weight polymer. Following 50 wt% PEI loading, both PEI-functionalized aerogels showed marked reductions in BET surface area and pore volume relative to pristine silica aerogel. The decrease was substantially greater for $PEI_{25,000}$–aerogel than for PEI_{600}–aerogel, indicating a stronger reduction in pore space available to nitrogen adsorption for the higher-molecular-weight polymer. Similar reductions in surface area and pore volume after amine/polymer incorporation have been reported for related porous silica systems [28,29]. The pore-size distributions nevertheless remained within the mesoporous range. The accompanying changes in surface chemistry were further examined using zeta-potential, FTIR, and TGA analyses.

3.1.2. Surface chemistry

3.1.2.1. Zeta potential. The zeta potential profiles **(**Fig. 1**d)** showed a clear change between pristine silica aerogels and the PEI-functionalized aerogels. The silica aerogel exhibited the expected negative surface charge across most of the tested pH range; the point of zero charge (pH_{PZC}) was found to be slightly below pH 5.0, with increasingly negative values at alkaline pH due to progressive deprotonation of surface silanol groups. This behavior is consistent with well-established silica surface chemistry [30].

PEI was impregnated within the silica aerogel rather than covalently grafted. Previous studies on PEI–silica systems have shown that PEI adsorption is governed primarily by electrostatic attraction between protonated amine groups and negatively charged silica surface sites, together with hydrogen-bonding interactions involving PEI amines and surface silanol groups [31].

Both PEI_{600} and $PEI_{25,000}$ silica aerogels showed positive surface potentials under acidic-to-neutral conditions, reflecting the protonation behavior of PEI amine groups [31–33]. Such charge reversal after PEI adsorption on silica has been reported previously [31]. $PEI_{25,000}$ aerogel remained more positively charged than PEI_{600} aerogel over most of the measured pH range, indicating a stronger positive surface character for the higher-molecular-weight PEI composite under acidic-to-neutral conditions.

3.1.2.2. Fourier transform infrared spectroscopy analysis. The FTIR spectra (Fig. 1**e**) highlight clear differences between the pristine and PEI-functionalized aerogels. The pristine silica aerogel is dominated by an absorption band at ~1080 cm^{-1}, which is characteristic of the asymmetric stretching vibration of Si–O–Si bonds in the siloxane network. After PEI functionalization, several new features appear that are not present in the pristine aerogel. These include a broad band in the 3400–3500 cm^{-1} region arising from overlapping N–H stretching modes (NH_x), a band near ~1570 cm^{-1} attributed to N–H bending vibrations, and a peak around ~2950 cm^{-1} corresponding to asymmetric C–H stretching of the PEI ethylene backbone. The emergence of these amine-related bands supports successful incorporation of PEI within the aerogel matrix. The spectra were baseline-corrected and presented on a common transmittance scale to enable direct comparison of the pristine and PEI-functionalized aerogels. Importantly, the Si–O–Si band remains clearly visible after functionalization, indicating that the silica framework is preserved after polymer incorporation [34,35].

3.1.2.3. Thermogravimetric analysis. TGA **(**Fig. 1**f)** was used to distinguish the inorganic and organic constituents within the aerogels. The

pristine silica aerogel exhibited minimal mass loss (< 4%), reflecting removal of adsorbed water and the thermal stability of the silica framework. In contrast, the PEI–silica aerogel showed a gradual decomposition profile. A small initial mass loss appeared below ~130 °C, corresponding to moisture removal, followed by a major degradation event between 250–450 °C linked to PEI thermal decomposition. The derivative thermogravimetric (DTG) inset showed a prominent peak in this temperature range, associated with thermal degradation of the PEI phase [36]. Beyond ~450 °C, the mass stabilized, with the remaining mass predominantly corresponding to the silica framework [37].

Taken together, the zeta-potential shift, PEI-associated FTIR bands, TGA mass-loss profile, and reduction in surface area and pore volume provide complementary evidence that PEI is incorporated within and the aerogel while the mesoporous structure is retained. Although these measurements do not resolve the molecular-scale spatial distribution of PEI, they indicate substantial modification of the aerogel surface environment by the impregnated polymer. The effects of PEI molecular weight on PFAS adsorption were subsequently evaluated.

3.2. Adsorption performance: kinetics and isotherm modelling

3.2.1. Comparative evaluation

Fig. 2**a** compares the equilibrium adsorption capacities of PFOA and PFBS on the pristine aerogel and PEI_{600} and $PEI_{25,000}$ aerogels, each prepared at 50 wt% PEI loading. The unmodified aerogel exhibits the lowest capacities, which is expected because its surface is mostly negatively charged and lacks functional groups that can interact strongly with anionic PFAS. After PEI functionalization, the uptake increases markedly for both PFOA and PFBS. This improvement reflects the presence of protonatable amines in PEI, which provide positively charged and polar sites that interact more favorably with PFAS headgroups. Between the two PEI loadings, the lower molecular weight PEI–silica aerogel shows the highest adsorption capacity (q_e). This agrees with the BET results, where higher molecular weight $PEI_{25,000}$ aerogel showed a greater reduction in surface area and pore volume than PEI_{600} aerogel. Based on the higher adsorption performance, PEI_{600} aerogel was selected for the subsequent adsorption experiments and is hereafter referred to as PEI aerogel.

3.2.2. Kinetic Studies

The adsorption kinetics of PFBS and PFOA on the PEI–silica aerogel (Fig. 2**b**) revealed rapid uptake, with equilibrium reached within approximately 60 min for PFBS and 120 min for PFOA. The sharp initial rise in adsorption during the first 10 min indicates rapid access to available adsorption sites on the PEI-modified aerogel surface. Kinetic modeling showed that for both PFBS and PFOA, the pseudo-second order (PSO) model provided the best fit ($R^2 > 0.99$) and the lowest RMSE, followed by the general order (GO) model and pseudo-first order (PFO) model. The PFO model underestimated the early-stage uptake, while the GO model also described the data reasonably well. The fitted kinetic parameters are summarized in Table S2. The good agreement with the PSO and GO models indicates that adsorption is strongly influenced by interactions at the PEI-functionalized surface [19,38–40].

These interactions may include electrostatic attraction between the protonated amine groups of PEI and the anionic sulfonate (PFBS) or carboxylate (PFOA) headgroups [41,42]. Hydrogen bonding and

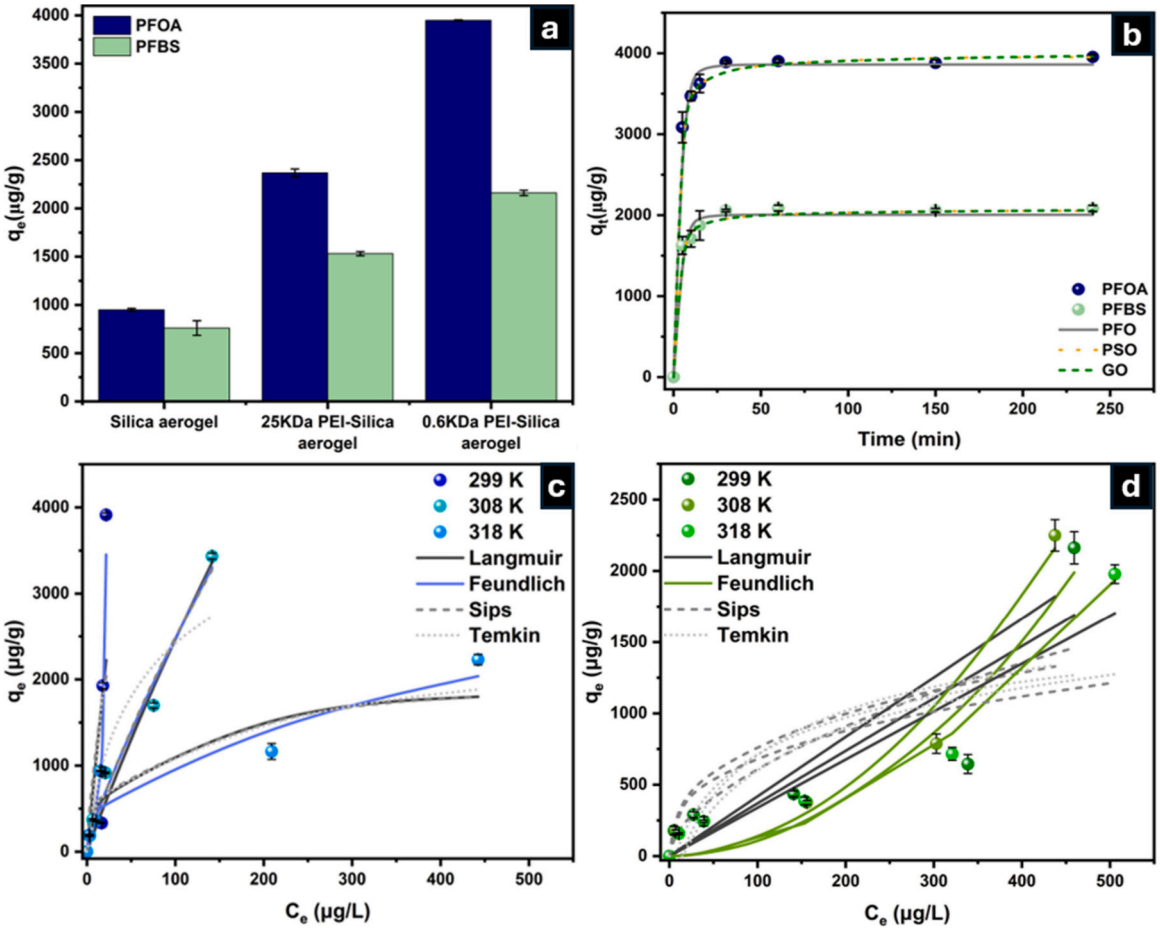

Fig. 2. Adsorption performance and model fitting for PFOA and PFBS: (a) effect of PEI molecular weight on adsorption capacity; (b) kinetic fits using pseudo-first order, pseudo-second order, and general-order models at an initial PFAS concentration of 1000 µg/L; and isotherm fits for (c) PFOA and (d) PFBS at 299, 308, and 318 K. All experiments were conducted at pH 6.5.

non-electrostatic interactions may also contribute, although their relative contributions cannot be resolved from kinetic fitting alone. PFOA exhibited a higher rate constant ($k_2 \approx 2.3 \times 10^{-3}$ g μg^{-1} h^{-1}) and greater adsorption capacity than PFBS, attributable to its longer perfluoroalkyl chain (C_8 vs. C_4), which enhances hydrophobic interactions and interfacial affinity. This chain-length-dependent behavior agrees with previous findings for amine- and carbon-based sorbents [43,44]. The Weber–Morris intraparticle diffusion plots showed an intermediate linear region with R^2 values of 0.938 and 0.978 for PFOA and PFBS, respectively (Figure S6). The corresponding intraparticle diffusion coefficient was higher for PFOA than for PFBS (k_{id} = 237.8 and 137.7 μg/g min$^{0.5}$, respectively). However, the substantial non-zero intercepts indicate that intraparticle diffusion was not the sole rate-controlling step and that boundary-layer transport also contributed to the overall adsorption kinetics. The equilibrium adsorption behavior of PFOA and PFBS was subsequently examined using adsorption isotherm models.

3.2.3. Isotherm studies

The equilibrium adsorption of PFOA and PFBS on PEI–silica aerogel was evaluated using Langmuir, Freundlich, Sips, and Temkin models across the temperature range of (299–318 K) (Fig. 2**c, d;** Table S3). Among the evaluated models, the Freundlich equation provided the best overall fit to of the experimental data, giving R^2 values (typically 0.899–0.982) and lowest RMSE other tested models (Table S3). The Freundlich fit indicates a heterogeneous distribution of adsorption sites within the PEI-functionalized aerogel. Similar Freundlich behavior has been reported by Tian *et al.* for PFOA adsorption on amino-functionalized graphene oxide aerogels, where the Freundlich model showed a better fit than Langmuir ($R^2 > 0.98$) [45].

The fitted Langmuir q_{max} at 299 K was higher for PFOA than for PFBS (1060.4 and 291.1 mg/g, respectively), in agreement with the greater uptake of PFOA observed experimentally. PFOA also showed stronger adsorption than PFBS across the investigated concentration range. The lower uptake of PFBS can be related to its shorter perfluoroalkyl chain, which reduces hydrophobic and interfacial contributions relative to PFOA [46]. Similar chain-length-dependent observations have been reported in previous PFAS adsorption studies, where long-chain PFAS generally show stronger affinity because electrostatic interactions are supplemented by hydrophobic and interfacial contributions from the fluorinated chain [47,48].

The Sips model did not improve the fit relative to Freundlich, while the Temkin model generally showed lower R^2 and higher RMSE values (Table S3), indicating a poorer fit of the equilibrium data over the studied concentration range. Overall, the isotherm results show heterogeneous adsorption behavior and a stronger affinity of the PEI aerogel toward PFOA than PFBS.

3.2.4. Thermodynamic interpretation

Thermodynamic parameters were estimated from the equilibrium adsorption data obtained at 299, 308, and 318 K. The corresponding van't Hoff plots and calculated parameters are provided in Figure S4 **and** Table S6. The Gibbs free-energy changes (ΔG°) were negative over the investigated temperature range, with values of approximately −27.2 to −28.3 kJ/mol for PFOA and −23.4 to −23.6 kJ/mol for PFBS, indicating thermodynamically favorable adsorption under the studied conditions.

The apparent enthalpy changes (ΔH°) were −11.0 kJ/mol for PFOA and −25.9 kJ/mol for PFBS, indicating an overall exothermic adsorption process for both compounds. Exothermic and spontaneous PFOA adsorption has also been reported for amino-functionalized graphene oxide aerogels, while similar behavior has been observed for PFOA/PFOS adsorption on chemically activated biomass and for PFOS adsorption on boehmite [45,49,50]. The corresponding entropy changes (ΔS°) were + 54.6 J/(mol·K) for PFOA and −7.9 J/(mol·K) for PFBS. The positive ΔS° for PFOA may reflect changes in hydration and release or rearrangement of interfacial water during adsorption, whereas the relatively small negative ΔS° for PFBS suggests only a limited decrease in interfacial disorder. Similar small negative entropy changes have been reported for PFOS adsorption on boehmite [49]. Previous studies on amino-functionalized adsorbents have shown that electrostatic attraction plays an important role in PFOA adsorption, while hydrophobic interactions become increasingly important with increasing PFAS chain length [45,50]. This agrees with the greater overall adsorption of PFOA compared with PFBS observed in the present study. The van't Hoff relationship showed a stronger linear correlation for PFBS ($R^2 \approx 0.98$) than for PFOA ($R^2 \approx 0.70$). The greater scatter for PFOA likely reflects the limited number of temperature points and variability in the equilibrium data.

3.2.5. Environmental Factors Affecting PFBS and PFOA Adsorption

The adsorption of PFOA and PFBS on the PEI–silica aerogel strongly depended on solution pH (Fig. 3**a**). Both compounds adsorbed best under acidic conditions (pH 3), with capacities exceeding ~3900 μg/g for PFOA and ~3000 μg/g for PFBS, then declined progressively as pH increased, reaching their lowest values at pH 9. This pH dependence reflects the influence of the protonation state of the PEI-functionalized surface controls adsorption. At low pH, PEI amine groups (pKa ≈ 6–10) are largely protonated, giving a positively charged surface that attracts the anionic headgroups of PFAS. As pH increases, deprotonation reduces surface charge density, weakening electrostatic attraction and lowering uptake. This trend points to a surface-charge-driven process rather than changes in PFAS speciation, since both PFOA and PFBS remain mostly anionic across the tested pH range. Differences between the two compounds emerged at higher pH. PFOA consistently adsorbed more than PFBS, likely due to its longer perfluoroalkyl chain (C_8 vs. C_4) and stronger hydrophobic contributions [43,51]. As electrostatic interactions diminish with decreasing surface protonation, adsorption increasingly relies on non-electrostatic contributions, which are inherently weaker for short-chain PFAS such as PFBS. Similar pH-dependent behavior has been reported for other amine-functionalized silica and carbon-based sorbents, where PFAS removal is maximized under acidic conditions and declines sharply near neutral to alkaline pH [19,41,42]. Overall, the pH-dependent results indicate that PEI protonation plays a major role in PFAS uptake, while chain-length-dependent non-electrostatic interactions help explain the higher retention of PFOA compared with PFBS.

Ionic strength strongly affected PFAS adsorption (Fig. 3b). With no added NaCl, both compounds reached maximum uptake (PFOA ≈ 4000 μg/g; PFBS > 2900 μg/g). Adding 10 or 100 mM NaCl sharply reduced adsorption, showing that uptake is sensitive to background electrolyte levels. Higher ionic strength compresses the electrical double layer around the protonated PEI surface, weakening electrostatic attraction between the positively charged amine sites and the anionic PFAS headgroups. Similar effects have been reported for other amine-modified sorbents [19,41]. At 100 mM NaCl, both compounds lost more than half of their adsorption capacity. PFOA still adsorbed more than PFBS across all ionic strengths, suggesting that hydrophobic interactions help retain PFOA even when electrostatic forces are suppressed. These non-electrostatic contributions do not fully offset the loss of attraction under high salt conditions. The stronger decrease observed for PFBS further supports its greater dependence on electrostatic interactions.

3.2.6. Adsorption performance in different water matrices

PEI aerogel showed different adsorption performance across water matrices **(**Fig. 4**)**. Key parameters for each matrix are listed in Table S1. In DI water, where background ion concentrations are minimal, the aerogel achieved near-complete removal of PFOA (98.8 ± 0.5%) and moderate removal of PFBS (54.8 ± 1.5%). Introducing dissolved ions into the system produced a systematic decline in PFAS uptake, following the order: river water (84.3 ± 11%) > tap water (79.5 ± 0.1%) > groundwater (69.8 ± 2.6%) ≈ STP effluent (68.8 ± 3.5%) for PFOA.

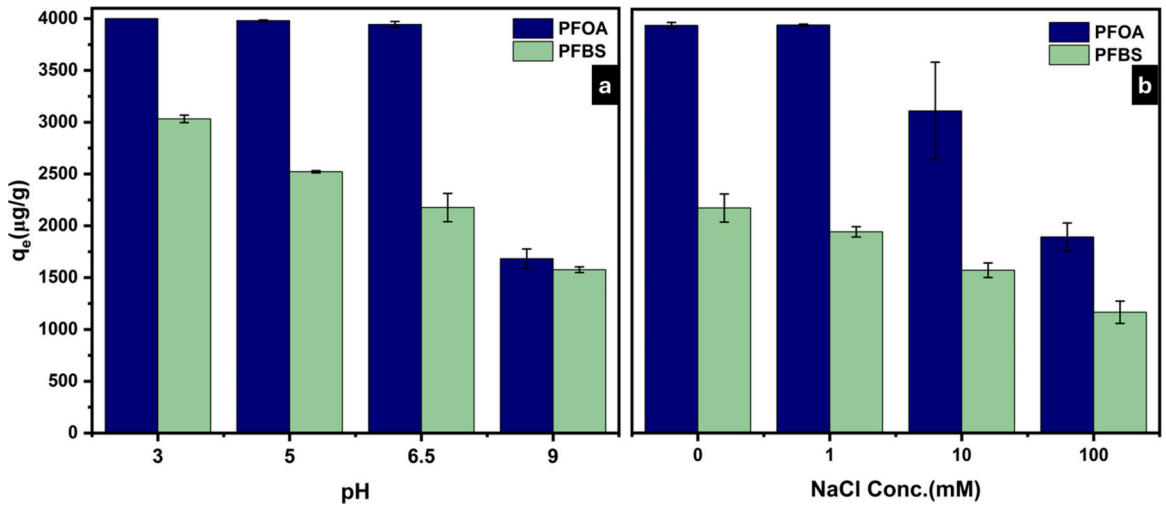

Fig. 3. Effect of pH and ionic strength on the adsorption of PFBS and PFOA by PEI–silica aerogel. Adsorption performance was determined under batch conditions in distilled water at 299 K. (a) Influence of pH (3–9) and (b) Influence of ionic strength (0–100 mM NaCl).

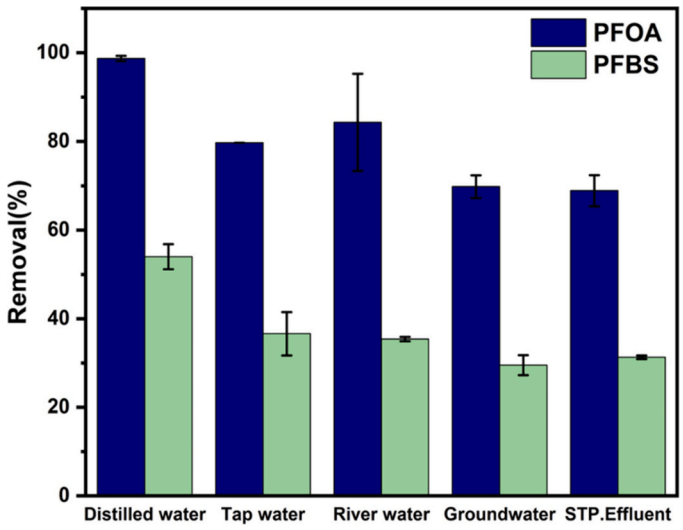

Fig. 4. Removal efficiency of PFOA and PFBS by PEI–silica aerogel in different water matrices, including distilled water, tap water, river water, groundwater, and sewage treatment plant (STP) effluent.

PFBS exhibited the same trend but with significantly lower overall removal (30–37%). These reductions generally follow the ionic strength gradients of the matrices: river water contained the lowest ionic strength (1.56×10^{-3} M), whereas the STP effluent exhibited the highest (1.41×10^{-2} M), dominated by chloride (240.58 mg/l), sulfate (82.88 mg/l), and substantial concentrations of Ca^{2+} and Mg^{2+}. Higher ionic strength compresses the electrostatic double layer around the protonated PEI surface, weakening attraction between the positively charged amine groups and anionic PFAS. Similar suppression of PFAS uptake on amine-functionalized sorbents at high electrolyte concentrations [20,52].

PFBS showed a stronger decrease in removal than PFOA in the high-ionic-strength matrices (groundwater and STP effluent). This stronger response likely reflects the shorter chain length of PFBS (C_4) and its greater dependence on electrostatic interactions [53]. PFOA, with its longer C_8 chain, can receive additional non-electrostatic contributions that help maintain higher removal even under competitive, high-salt conditions [20,53,54]. Similar chain-length effects have been reported for amine-rich polymers and silica adsorbents, where long-chain PFCAs show greater adsorption than short-chain ones in saline water [55]. The influence of dissolved organic matter on PFAS adsorption has also been demonstrated experimentally. Humic acid significantly suppressed PFBS and PFOS sorption through competitive surface interactions, with short-chain PFBS showing particularly strong sensitivity to organic matter [56]. Similarly, humic-acid coverage of mineral surfaces, including SiO_2, was shown to substantially reduce PFOA adsorption by limiting available sorption sites [57]. Because dissolved organic matter was not quantified in the present matrices, its specific contribution could not be separated from the overall matrix effect.

3.2.7. *Desorption, reusability, and stability of PEI–aerogels*

The desorption and reusability of PEI–aerogels were investigated using different desorption agents and successive adsorption–desorption cycles to evaluate both PFAS release efficiency and retention of adsorption performance (Fig. 5**a**). The selected stripping solvents 80% isopropanol (IPA) [20], 80% methanol (MeOH) [20], 1% NaCl in 80% IPA, and 1% NaCl in 80% MeOH [20] were chosen based on previous studies demonstrating high desorption efficiency of PFAS from loaded sorbents [41]. Among these, 1% NaCl in 80% MeOH showed the highest desorption efficiency, reaching ~97% for PFOA and ~85% for PFBS [20,58]. This improved desorption likely results from the combined effect of methanol and salt: methanol weakens PFAS–surface interactions by lowering the polarity of the desorption medium, while chloride ions can compete with adsorbed PFAS anions at protonated amine sites [41]. In contrast, when IPA or MeOH alone was used, only 45–55% desorption was achieved, indicating that solvent polarity alone was not sufficient to fully release adsorbed PFAS under the tested conditions.

Five consecutive adsorption–desorption cycles were then performed using the best regenerant (1% NaCl in 80% MeOH). Between cycles, the aerogel was dried at 65 °C for 3 h. PFOA removal dropped from ~97% in the first cycle to ~88% after the fifth, and PFBS from ~85% to ~75% (Fig. 5**b**). The slight loss in efficiency may result from incomplete desorption, partial pore blockage, or reduced availability of protonated amine sites after repeated wetting, drying, and reuse, as reported for other amine-functionalized adsorbents [20,42]. To further evaluate the stability of the impregnated PEI phase, TGA was performed on aerogels recovered after exposure to different pH conditions and after repeated adsorption–desorption cycles (Figure S5). The recovered materials retained a clear PEI-associated thermal degradation contribution across the investigated pH range and after five cycles, indicating that a substantial organic fraction remained associated with the silica support, although changes in the mass-loss profiles suggest that some redistribution or loss of PEI cannot be excluded. The relatively stable removal over five cycles suggests that PFAS adsorption on the PEI–silica surface is at least partly reversible under the selected laboratory desorption

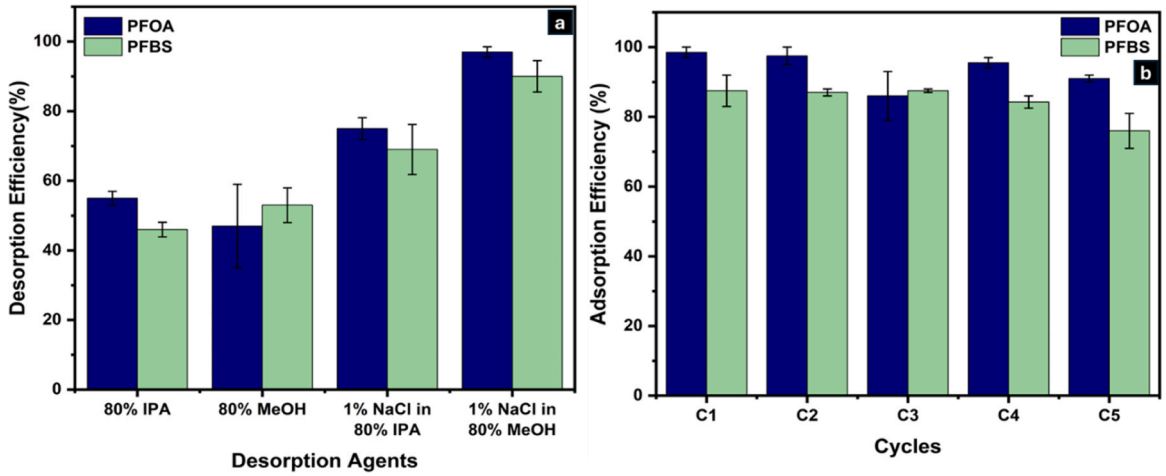

Fig. 5. Desorption and reusability performance of PEI–aerogel for PFOA and PFBS: (a) desorption efficiency using 80% isopropanol, 80% methanol, 1% NaCl in 80% isopropanol, and 1% NaCl in 80% methanol; and (b) adsorption efficiency over five adsorption–desorption cycles using 1% NaCl in 80% methanol. Conditions: initial PFAS concentration = 1000 μg/L, solution volume = 40 mL, adsorbent mass = 10 mg.

conditions. While electrostatic interactions, hydrogen bonding, and non-electrostatic interactions may all contribute to PFAS retention, their relative contributions cannot be fully resolved from the desorption experiments alone [59–61].

Overall, the combination of effective regeneration efficiency and retention of adsorption performance over repeated cycles demonstrates the reusability of the PEI aerogel under the tested conditions. The 80% MeOH–1%NaCl regenerant provided effective regeneration under the tested conditions while maintaining sorbent efficiency over repeated cycles. However, because PEI is physically impregnated rather than covalently grafted, some polymer loss during aqueous exposure cannot be excluded, and future studies should evaluate direct PEI leaching and more permanent immobilization strategies.

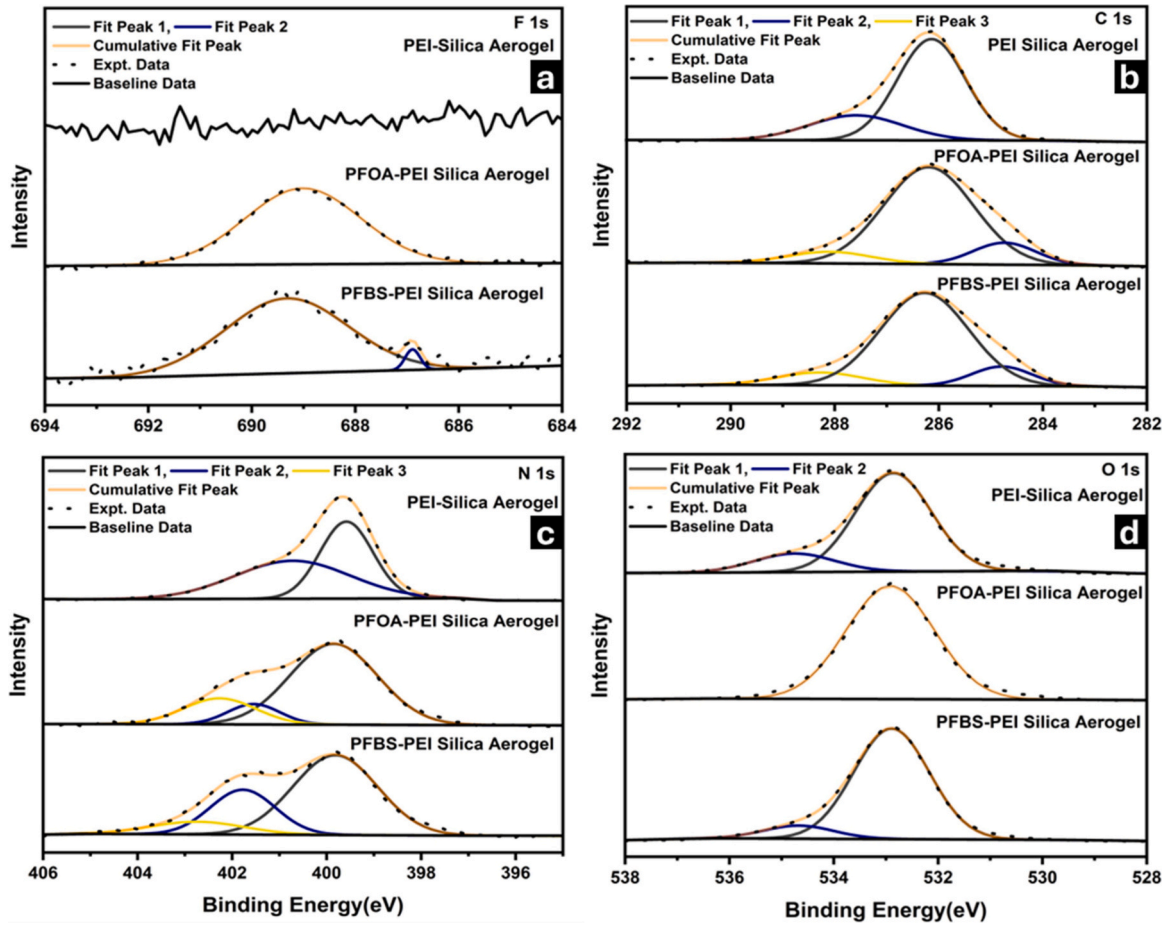

Fig. 6. High-resolution XPS spectra of PEI–silica aerogel before and after adsorption of PFOA and PFBS: (a) F 1 s, (b) C 1 s, (c) N 1 s, and (d) O 1 s regions.

4. Mechanistic Insight

To further examine PFAS retention on the PEI–silica aerogel, XPS was used to evaluate changes in surface composition and chemical states before and after adsorption. A clear indication of PFAS retention appears in the F 1 s region **(**Fig. 6**a)**. The untreated aerogel contains no detectable fluorine, whereas both PFOA- and PFBS-loaded samples develop a distinct peak at ~689–690 eV. Survey-spectrum quantification showed F contents of 1.99 and 0.61 at% for the PFOA- and PFBS-loaded aerogels, respectively, corresponding to F/C ratios of approximately 0.116 and 0.035. The higher surface fluorine content after PFOA adsorption closely correlates with the greater PFOA adsorption measured in the adsorption experiments. This binding-energy range is commonly assigned to CF_2/CF_3 groups and has also been reported for PFBS bound to PEI/CS xerogels [62]. Similar F 1 s features have also been reported for PFAS captured on quaternary-amine-modified graphene oxide and other functionalized sorbents [63]. The PFBS spectrum additionally exhibits a small lower-BE shoulder, which may reflect a more heterogeneous fluorine environment after PFBS adsorption.

Further changes in the surface chemical environment are evident from the C 1 s spectra **(**Fig. 6**b)**. The pristine aerogel is dominated by a C–C/C–N peak at ~285 eV, while changes are observed in the higher-binding-energy region following PFAS adsorption. Because carbon contributions around ~288–289 eV may overlap, this feature is not assigned exclusively to fluorinated carbon. For comparison, fluorinated carbon components at higher binding energies (~291–294 eV) have been reported for PFOA adsorption on MO_V–CNT hybrids [64]. Therefore, the C 1 s changes are considered complementary to the more direct evidence of PFAS retention provided by the F 1 s spectra.

The XPS N 1 s spectra **(**Fig. 6**c)** provide insight into changes in the chemical environment of PEI following PFAS adsorption. The pristine PEI-aerogel contains both neutral and protonated amine environments. Quantitative N 1 s fitting showed a redistribution of the nitrogen chemical-state contributions after PFOA and PFBS adsorption, including higher-binding-energy components associated with changes in the local environment of PEI amine groups (Table S4). Similar changes in nitrogen chemical states have been reported for PFAS adsorption on amine-containing sorbents [62,63]. In the present system, the N 1 s changes are indicative of the involvement of PEI amine sites in interactions with anionic PFAS headgroups.

By contrast, the O 1 s spectra **(**Fig. 6**d)** remain dominated by silica-related oxygen and show only minor changes, which is consistent with the literature where PFAS oxygen states often overlap with strong Si–O or C–O signals in hybrid materials. A summary of XPS peak positions and together with the quantitative surface composition and N 1 s speciation is provided in Table S4, and the corresponding XPS survey and FTIR spectra are shown in Figure S1.

Overall, the XPS results support the retention of both PFOA and PFBS on the PEI–silica aerogel surface. The appearance and quantitative abundance of surface fluorine provide direct evidence of PFAS retention, while the changes in the N 1 s region support the involvement of PEI amine groups during adsorption. The higher F/C ratio of the PFOA-loaded aerogel also closely correlates with the greater PFOA adsorption observed in the adsorption experiments. These surface signatures support the adsorption trends discussed above, where electrostatic interactions contribute strongly to uptake, while chain-length-dependent non-electrostatic interactions help explain the higher retention of PFOA relative to PFBS.

The post-adsorption FTIR spectra (Figure S1) retained the principal PEI–silica bands, while modest changes in the PEI-associated regions were observed after PFOA and PFBS adsorption. In particular, changes in the ~1500–1650 cm^{-1} region suggest modification of the local environment of amine-containing groups, while the dominant Si–O–Si band remained evident. These FTIR changes provide complementary evidence of PFAS–PEI interaction, whereas XPS provides the more direct evidence of PFAS retention on the surface.

5. Conclusion

This study demonstrates a microemulsion-assisted sol–gel strategy for producing mesoporous silica aerogel particles functionalized with polyethyleneimine (PEI), providing a tunable platform for PFAS adsorption. The synthesis retained a partly accessible mesoporous framework after PEI incorporation, allowing the relationship between pore accessibility, amine functionality, and PFAS uptake to be examined. A key outcome is the identification of PEI molecular weight as a critical design parameter. Lower-molecular-weight PEI improved PFAS uptake by preserving mesopore accessibility and causing less restriction of the pore structure, whereas higher-molecular-weight PEI led to partial pore filling and reduced effective adsorption capacity. These results highlight the need to balance functional-group density with accessible pore volume when designing amine-based PFAS sorbents.

Adsorption was rapid for both PFOA and PFBS, with equilibrium reached within 60–120 min, indicating that the PEI-functionalized aerogel provides readily accessible adsorption sites under the tested batch conditions. Across controlled conditions and selected water matrices, PFOA removal remained comparatively higher than PFBS removal, while PFBS showed greater sensitivity to pH and ionic strength, particularly in ion-rich groundwater and sewage treatment plant effluent. These differences reflect chain-length-dependent adsorption behavior: PFBS adsorption appears to depend more strongly on electrostatic interactions, whereas PFOA benefits from additional non-electrostatic contributions associated with its longer perfluoroalkyl chain. The PEI–silica aerogels retained a substantial fraction of their initial removal efficiency over five adsorption–desorption cycles, indicating partial reversibility and reuse potential under laboratory desorption conditions. However, the greater performance loss observed for PFBS indicates that regeneration and reuse strategies require further optimization.

From an application perspective, the PEI-functionalized silica aerogel may be considered as a candidate polishing-stage adsorbent for PFAS removal, particularly where additional treatment is required after primary removal processes. In such systems, it could potentially complement or serve as an alternative to activated-carbon-based polishing media, especially when selective amine–PFAS interactions and adsorbent regeneration are advantageous. Nevertheless, practical implementation will require conversion of the powder into mechanically stable shaped or immobilized forms, together with evaluation of hydraulic performance, service life, regeneration efficiency, and cost relative to established activated carbon and ion-exchange systems. Further work should extend the evaluation to broader PFAS mixtures, lower environmentally relevant concentration ranges, dissolved organic matter-containing matrices, shaped or immobilized adsorbent forms, and continuous-flow column operation.

Overall, the mechanistic insights gained in this study support the rational design of improved PFAS sorbents, particularly by showing how PEI molecular weight and accessibility within a fibrous silica aerogel framework influences long- and short-chain PFAS adsorption. By contributing to the development of reusable sorbents for PFAS removal, this work is relevant to broader efforts aligned with the United Nations Sustainable Development Goals, particularly SDG 6 on clean water and sanitation, with indirect relevance to SDG 3 on good health and well-being and SDG 12 on responsible consumption and production.

CRediT authorship contribution statement

Jai Kishan Rajak: Writing – original draft, Visualization, Investigation, Formal analysis, Data curation, Conceptualization. **G.V. Koulini:** Writing – review & editing, Methodology, Investigation. **Indumathi M. Nambi:** Writing – review & editing, Supervision, Resources, Funding acquisition, Conceptualization. **Sulalit Bandyopadhyay:** Writing – review & editing, Supervision, Resources, Project administration, Funding acquisition.

Declaration of Generative AI and AI-assisted technologies in the writing process

During the manuscript writing of this work, the authors used ChatGPT (4.1) and Gemini to improve the language, clarity, and readability of the manuscript. After using this tool, the authors reviewed and edited the content as needed and take full responsibility for the content of the published article.

Declaration of Competing Interest

The authors declare that they have no known competing financial interests or personal relationships that could have appeared to influence the work reported in this paper.

Acknowledgement

The authors also acknowledge the Department of Civil Engineering (Environmental Engineering Division, Department of Civil Engineering), Indian Institute of Technology Madras (IIT Madras), where the adsorption experiments and analytical measurements were conducted. Financial support from the Indian Council of Medical Research (ICMR), Government of India, is gratefully acknowledged through Project No. CIE/1819/273/ICMR/INDU for the procurement of the LC–MS/MS facility used in this study. The authors further acknowledge Funder Name: The Norwegian Directorate for Higher Education and Skills through project INCP2–2024/10214 - Fostering Safety in Use of Advanced Nanomaterials in Health Sector for financially supporting Jai Kishan Rajak during his stay at IIT Madras. Technical assistance with centrifugation, shaker incubator facilities, and water sampling is gratefully acknowledged, including support from S. S. Sasidharan and Vaibhav Kabdwal. The authors gratefully acknowledge the Particle Engineering Centre, Department of Chemical Engineering, Norwegian University of Science and Technology (NTNU), where the synthesis and functionalization of the silica aerogels were carried out. The authors thank NTNU for providing laboratory infrastructure and technical support, and acknowledge the Research Council of Norway for supporting the Norwegian Micro- and Nano-Fabrication Facility (NorFab) under Project No. 295864. Access to nitrogen physisorption (BET) instrumentation was provided by the Department of Materials Science at NTNU.

Appendix A. Supporting information

Supplementary data associated with this article can be found in the online version at doi:10.1016/j.jece.2026.125663.

Data Availability

Data will be made available on request.

References

[1] H. Brunn, et al., PFAS: forever chemicals—persistent, bioaccumulative and mobile. Reviewing the status and the need for their phase out and remediation of contaminated sites, Environ. Sci. Eur. 35 (1) (2023) 1–50.
[2] F. Xiao, et al., Cross-national challenges and strategies for PFAS regulatory compliance in water infrastructure, Nat. Water 1 (12) (2023) 1004–1015.
[3] M.G. Evich, et al., Per- and polyfluoroalkyl substances in the environment, Science 375 (6580) (2022) eabg9065.
[4] O, Reconciling Terminology of the Universe of Per- and Polyfluoroalkyl Substances: Recommendations and Practical Guidance. OECD Series on Risk Management of Chemicals, OECD Publishing, Paris, 2021.
[5] J. Glüge, et al., An overview of the uses of per-and polyfluoroalkyl substances (PFAS), Environmental Science Processes & Impacts 22 (12) (2020) 2345–2373.
[6] G. Munoz, et al., Bioaccumulation and trophic magnification of emerging and legacy per-and polyfluoroalkyl substances (PFAS) in a St. Lawrence River food web, Environ. Pollut. 309 (2022) 119739.
[7] Y. Vasseghian, et al., A global meta-analysis of phthalate esters in drinking water sources and associated health risks, Sci. Total. Environ. 903 (2023) 166846.
[8] K.E. Pelch, T. McKnight, A. Reade, 70 analyte PFAS test method highlights need for expanded testing of PFAS in drinking water, Sci. Total. Environ. 876 (2023) 162978.
[9] M. Hamza, et al., Understanding PFAS Adsorption: How Molecular Structure Affects Sustainable Water Treatment, Environments 12 (9) (2025) 330.
[10] L.G. Gaines, Historical and current usage of per-and polyfluoroalkyl substances (PFAS): A literature review. Am. J. Ind. Med. 66 (5) (2023) 353–378.
[11] H. Mahoney, et al., Next generation per-and poly-fluoroalkyl substances: Status and trends, aquatic toxicity, and risk assessment, Eco-Environ. & Health 1 (2) (2022) 117–131.
[12] K.A. Coates, P.d.B. Harrington, Contamination levels of per- and polyfluoroalkyl substances (PFAS) in recent North American precipitation events. A review, Water Res. 266 (2024) 122390.
[13] P.J. Brahana, R. Patel, B. Bharti, Surface science view of perfluoroalkyl acids (PFAAs) in the environment, ACS Environ. Au 4 (4) (2024) 173–185.
[14] S. Sun, et al., Occurrence and profiles of perfluoroalkyl substances in wastewaters of chemical industrial parks and receiving river waters: Implications for the environmental impact of wastewater discharge, Sci. Total. Environ. 945 (2024) 173993.
[15] S.M. Thagard, Focusing water treatment efforts on the destruction of poly-and perfluoroalkyl substances (PFAS): the United States perspective, Clean. Technol. Environ. Policy 24 (6) (2022) 1619–1620.
[16] T. Schroeder, D. Bond, J. Foley, PFAS soil and groundwater contamination via industrial airborne emission and land deposition in SW Vermont and Eastern New York State, USA. Environmental Science Processes & Impacts 23 (2) (2021) 291–301.
[17] S.J. Amirfakhri, et al., Enhanced PFBS adsorption via silver-impregnated activated carbon: Mechanistic insights and Thermodynamic analysis, Chemosphere 375 (2025) 144257.
[18] M. Zhang, et al., Cutting-edge technologies and relevant reaction mechanism difference in treatment of long-and short-chain per-and polyfluoroalkyl substances: a review, Chemosphere 354 (2024) 141692.
[19] X. Lei, et al., A review of PFAS adsorption from aqueous solutions: Current approaches, engineering applications, challenges, and opportunities, Environ. Pollut. 321 (2023) 121138.
[20] E. Gagliano, et al., Removal of poly- and perfluoroalkyl substances (PFAS) from water by adsorption: Role of PFAS chain length, effect of organic matter and challenges in adsorbent regeneration, Water Res. 171 (2020) 115381.
[21] P. Punyapalakul, et al., Effects of surface functional groups and porous structures on adsorption and recovery of perfluorinated compounds by inorganic porous silicas, Sep. Sci. Technol. 48 (5) (2013) 775–788.
[22] F. Qin, et al., Polyethyleneimine functionalized cellulose-rich agroforestry residues for removing perfluorooctanoic acid: adsorption performance and mechanism, Cellulose 30 (6) (2023) 3653–3666.
[23] V. Polshettiwar, et al., High-Surface-Area Silica Nanospheres (KCC-1) with a Fibrous Morphology, Angew. Chem. Int. Ed. 49 (50) (2010) 9652–9656.
[24] Q.K.T. Doan, K.Y. Chiang, Facile synthesis of polyethyleneimine-modified cellulose nanocrystal/silica hybrid aerogel for CO2 adsorption, Environ. Sci. Pollut. Res. 32 (6) (2025) 3438–3455.
[25] N. Hüsing, U. Schubert, Aerogels-Airy Materials: Chemistry, Structure, and Properties, Angew. Chem. Int. Ed. Engl. 37 (1-2) (1998) 22–45.
[26] A.C. Pierre, G.M. Pajonk, Chemistry of Aerogels and Their Applications, Chem. Rev. 102 (11) (2002) 4243–4266.
[27] D. Ge, et al., Hydrophobic and thermal insulation properties of silica aerogel/epoxy composite, J. Non-Cryst. Solids 355 (52) (2009) 2610–2615.
[28] M. Nassi, et al., Removal of perfluorooctanoic acid from water by adsorption on high surface area mesoporous materials, J. Porous Mater. 21 (4) (2014) 423–432.
[29] F.A. Hussain, et al., Adsorption of perfluorooctanoic acid from water by pH-modulated Brönsted acid and base sites in mesoporous hafnium oxide ceramics, iScience 25 (4) (2022) 104138.
[30] L. Tzounis, et al., Controlled growth of Ag nanoparticles decorated onto the surface of SiO2 spheres: a nanohybrid system with combined SERS and catalytic properties, RSC Adv. 4 (34) (2014) 17846–17855.
[31] B.C. Ong, Y.K. Leong, S.B. Chen, Interparticle forces in spherical monodispersed silica dispersions: Effects of branched polyethylenimine and molecular weight, J. Colloid Interface Sci. 337 (1) (2009) 24–31.
[32] J.D. Ziebarth, Y. Wang, Understanding the protonation behavior of linear polyethylenimine in solutions through Monte Carlo simulations, Biomacromolecules 11 (1) (2010) 29–38.
[33] R. Mészáros, et al., Adsorption and Electrokinetic Properties of Polyethylenimine on Silica Surfaces, Langmuir 18 (16) (2002) 6164–6169.
[34] K. Choi, et al., Chromium removal from aqueous solution by a PEI-silica nanocomposite, Sci. Rep. 8 (1) (2018) 1438.
[35] H. Ahmad, et al., Preconcentration and speciation of arsenic by using a graphene oxide nanoconstruct functionalized with a hyperbranched polyethyleneimine, Microchim. Acta 185 (6) (2018) 290.
[36] Z. Zhang, et al., Development of silica-gel-supported polyethylenimine sorbents for CO2 capture from flue gas, AIChE J. 58 (8) (2012) 2495–2502.
[37] K. Li, et al., The influence of polyethyleneimine type and molecular weight on the CO2 capture performance of PEI-nano silica adsorbents, Appl. Energy 136 (2014) 750–755.
[38] M. Hubbe, S. Azizian, S. Douven, Implications of apparent pseudo-second-order adsorption kinetics onto cellulosic materials: A review, BioResources 14 (2019) 7582–7626.

[39] H. Son, B. An, Investigation of Adsorption Kinetics for Per- and Poly-fluoroalkyl substances (PFAS) Adsorption onto Powder Activated Carbon (PAC) in the Competing Systems, Water Air & Soil. Pollut. 233 (4) (2022) 129.
[40] D. Li, et al., Efficient removal of short-chain and long-chain PFAS by cationic nanocellulose, J. Mater. Chem. A 11 (18) (2023) 9868–9883.
[41] M. Ateia, et al., Efficient PFAS Removal by Amine-Functionalized Sorbents: Critical Review of the Current Literature, Environ. Sci. & Technol. Lett. 6 (12) (2019) 688–695.
[42] A. Lamy-Mendes, et al., Amine Modification of Silica Aerogels/Xerogels for Removal of Relevant Environmental Pollutants, Molecules 24 (20) (2019).
[43] A. Valencia, et al., Comparing the removal and fate of long and short chain per- and polyfluoroalkyl substances (PFAS) during surface water treatment via specialty adsorbents, J. Water Process. Eng. 56 (2023) 104345.
[44] G. Kim, D.N. Mengesha, Y. Choi, Adsorption dynamics of per- and polyfluoroalkyl substances (PFAS) on activated carbon: Interplay of surface chemistry and PFAS structural properties, Sep. Purif. Technol. 349 (2024) 127851.
[45] D. Tian, et al., Removal of perfluorooctanoic acid (PFOA) from aqueous solution by amino-functionalized graphene oxide (AGO) aerogels: Influencing factors, kinetics, isotherms, and thermodynamic studies, Sci. Total. Environ. 783 (2021) 147041.
[46] M. Riegel, B. Haist-Gulde, F. Sacher, Sorptive removal of short-chain perfluoroalkyl substances (PFAS) during drinking water treatment using activated carbon and anion exchanger, Environ. Sci. Eur. 35 (1) (2023) 12.
[47] M. Sadia, et al., Sorption of per- and poly-fluoroalkyl substances and their precursors on activated carbon under realistic drinking water conditions: Insights into sorbent variability and PFAS structural effects, Heliyon 10 (2024).
[48] S.B. Kang, et al., Removal of short- and long-chain PFAS from aquatic systems using electrostatic attraction of polyethylenimine-polyvinyl chloride electrospun nanofiber adsorbent, Sep. Purif. Technol. (2023).
[49] J. Qian, et al., Co-adsorption of perfluorooctane sulfonate and phosphate on boehmite: Influence of temperature, phosphate initial concentration and pH, Ecotoxicol. Environ. Saf. 137 (2017) 71–77.
[50] A.V. Alves, M. Tsianou, P. Alexandridis, Fluorinated Surfactant Adsorption on Mineral Surfaces: Implications for PFAS Fate and Transport in the Environment, Surfaces 3 (2020) 516–566, https://doi.org/10.3390/surfaces3040037.
[51] Y. He, et al., Advancing PFAS Sorbent Design: Mechanisms, Challenges, and Perspectives, ACS Mater. Au 4 (2) (2024) 108–114.
[52] O. Dudarko, et al., Removal of Poly- and Perfluoroalkyl Substances from Natural and Wastewater by Tailored Silica-Based Adsorbents, ACS ES&T Water 4 (4) (2024) 1303–1314.
[53] X. Min, Y. Wang, Enhanced adsorption of short-chain perfluorobutanoic acid by functionalized periodic mesoporous organosilica: Performance and mechanisms, J. Hazard. Mater. 449 (2023) 131047.
[54] S.B. Kang, et al., Removal of short- and long-chain PFAS from aquatic systems using electrostatic attraction of polyethylenimine-polyvinyl chloride electrospun nanofiber adsorbent, Sep. Purif. Technol. 326 (2023) 124853.
[55] A. Imran, et al., Adsorption of PFCAs using polyethyleneimine modified Biochar: Role of chain length and effects of water matrices, Chemosphere 386 (2025) 144650.
[56] F. Wang, K. Shih, J.O. Leckie, Effect of humic acid on the sorption of perfluorooctane sulfonate (PFOS) and perfluorobutane sulfonate (PFBS) on boehmite, Chemosphere 118 (2015) 213–218.
[57] K.H. Yang, et al., Role of Dissolved Organic Matter in Sorption of Perfluorooctanoic Acid to Metal Oxides, Water Environ. Res. 88 (8) (2016) 779–784.
[58] Z. Ren, et al., Combination of adsorption/desorption and photocatalytic reduction processes for PFOA removal from water by using an aminated biosorbent and a UV/sulfite system, Environ. Res. 228 (2023) 115930.
[59] A.K. Ilango, et al., Surface-modified biopolymers for removing mixtures of per- and polyfluoroalkyl substances from water: Screening and removal mechanisms, Environ. Pollut. (2023) 121865.
[60] A.K. Ilango, et al., Experimental and density functional theory investigation of surface-modified biopolymer for improved adsorption of mixtures of per- and polyfluoroalkyl substances in water, Water Res. 255 (2024) 121458.
[61] M. Chen, et al., Preparation of amino-modified cellulose aerogels and adsorption on typical diclofenac sodium contaminant, Environ. Sci. Pollut. Res. 29 (2021) 19790–19802.
[62] M.R. Shirzad Kebria, et al., Efficient removal of perfluorobutanesulfonic acid from water through a chitosan/polyethyleneimine xerogel, Chem. Eng. J. 466 (2023) 143236.
[63] M.N. Pervez, et al., Surface Modification of Graphene Oxide for Fast Removal of Per- and Polyfluoroalkyl Substances (PFAS) Mixtures from River Water, ACS ES&T Water 4 (7) (2024) 2968–2980.
[64] M. Lu, et al., Mechanochemical mineralization of “very persistent” fluorocarbon surfactants - 6:2 fluorotelomer sulfonate (6:2FTS) as an example. Sci. Rep. 7 (1) (2017) 17180.